

An Analytical Investigation of the Trapeze Effect Acting on a Thin Flexible Ribbon

Jérôme F. Sicard¹

Research Associate
Department of Aerospace Engineering
and Engineering Mechanics,
The University of Texas at Austin,
Austin, TX 78712
e-mail: jerome.sicard@utexas.edu

Jayant Sirohi

Associate Professor
Department of Aerospace Engineering
and Engineering Mechanics,
The University of Texas at Austin,
Austin, TX 78712
e-mail: jayant.sirohi@mail.utexas.edu

This paper systematically explores the extensional–torsional coupling due to the trapeze effect acting on a thin flexible ribbon subjected to combined tension and torsion. Kinematic relationships as well as expressions for the restoring torque associated with this effect are analytically derived. Additionally, the locus of points about which the cross sections of a twisted ribbon under tension rotate is derived. These points, called torsional centers, are found to be coincident with the centroids of the axial stress field at each station along the ribbon. More generally, it is shown that when a flexible slender member is in tension, combined transverse forces must act at the centroid of the axial stress field to produce pure bending and no twist. As a result, the elastic axis (EA) of the member shifts from the locus of shear centers to the locus of centroids of the axial stress field. A numerical model is developed to investigate the effect of the position of the EA on the prediction of steady-state deformations and natural frequencies of a rotating ribbon with tip mass. By assuming the EA to be the locus of the shear centers, the tip twist is overpredicted by a factor of 2 for small twist angles, and up to 2.5 for large twist deformations. In addition, assuming the EA to be the locus of shear centers results in an error of up to 60% in the predicted natural frequencies at large twist angles. [DOI: 10.1115/1.4028781]

1 Introduction

The trapeze effect, or bifilar effect, can be described as the tendency of a member subjected to an axial load to resist torsion. Or equivalently, it is the tendency of a pretwisted member to untwist under the action of an axial load. This effect was first observed experimentally by Campbell [1] and Pealing [2], who studied the torsional rigidity of phosphor bronze strips in vibration galvanometers. The first theoretical explanation was given by Buckley [3], who showed that the geometric change of direction of the twisted fibers of a member induces a foreshortening responsible for the increase in torsional rigidity. Relying on this result, referred to as “Buckley’s hypothesis,” rotor dynamicists developed equations to analytically capture the increase in torsional rigidity caused by centrifugal forces acting on rotor blades. Of particular significance are the works by Houbolt and Brooks [4], Fulton and Hodges [5], and Kaza and Kielb [6]. More recently, general purpose treatments of the effect were offered by researchers such as Borri and Merlini [7] following an initial-stress approach, and Popescu and Hodges [8] using a non-linear asymptotic analysis. A comprehensive literature review on the trapeze effect can be found in Ref. [9].

The extensional–torsional coupling resulting from the trapeze effect plays an important role in the torsional dynamics of ribbons with negligible structural stiffness, experiencing large torsional deformations. In this paper, the contribution of the trapeze effect to the torsional dynamics of thin flexible ribbons is explored analytically. First, the kinematic relationship and restoring torque associated with the trapeze effect are derived. Then, the spanwise locus of points, called torsional centers, about which the cross sections of a twisted ribbon rotate when it is subjected to an axial load is derived. The curve connecting the torsional centers is the torsional axis. Finally, the general case of combined axial load, transverse load, and torque acting on a flexible ribbon is

considered. The locus of points at which transverse loads must be applied to induce bending only, called elastic centers, is investigated. In addition, a numerical model is derived to investigate the influence of the position of the EA on the prediction of deformation and natural frequencies.

2 Physical Principles

In this section, the coupled extensional–torsional kinematic relationships associated with the trapeze effect are derived. In addition, the expression for the restoring torque arising from this effect is formulated. Finally, the position of the torsional axis is investigated.

2.1 Kinematics

2.1.1 Classical Trapeze. To describe the kinematics of the trapeze effect, it is natural to consider first the extension–torsion behavior of a simple trapeze, consisting of a rigid bar suspended from its ends by inextensible cables (see Fig. 1). The width of the undeformed trapeze is c and the length of the cables is R . When twisted, the tip of the trapeze makes an angle relative to the root equal to θ . Because the cables are inextensible, the twisting results in a shortening of the trapeze by an amount u_F ; this displacement is called axial foreshortening. Points P and Q , at distances equal to x and R , respectively, from the root, displace to P' and Q' after deformation. The expression for the variation of the axial displacement u_F as a function of the tip twist angle θ is derived below.

The position of P' relative to A , projected in the Newtonian coordinate system $\{x, y, z\}$, is given by

$$\mathbf{AP}' = (x - u_F(x))\mathbf{i} + \left(y_{P'} - \frac{c}{2}\right)\mathbf{j} + z_{P'}\mathbf{k} \quad (1)$$

where \mathbf{i} , \mathbf{j} , and \mathbf{k} are unit vectors directed along the x , y , and z -directions, respectively. In addition, because the cables forming the trapeze are inextensible, it can be deduced that

$$\|\mathbf{AP}'\| = \|\mathbf{AP}\| = x \quad (2)$$

¹Corresponding author.

Contributed by the Applied Mechanics Division of ASME for publication in the JOURNAL OF APPLIED MECHANICS. Manuscript received July 20, 2014; final manuscript received October 8, 2014; accepted manuscript posted October 10, 2014; published online October 30, 2014. Assoc. Editor: George Kardomateas.

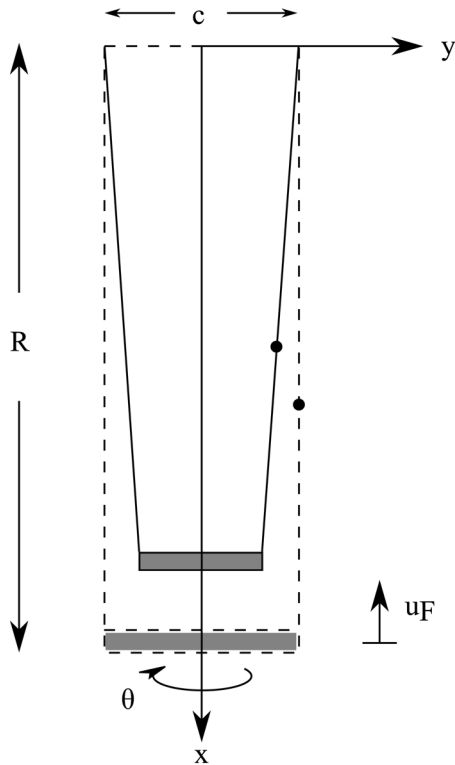


Fig. 1 Undeformed (dashed lines) and deformed (solid lines) shape of a trapeze in torsion

Combining Eqs. (1) and (2), a quadratic equation in u_F is obtained. Only one of the two roots of this polynomial is physically meaningful. This root is given by

$$u_F(x) = x - \sqrt{x^2 - y_{P'}^2 - z_{P'}^2 - \frac{c^2}{4} + cy_{P'}} \quad (3)$$

Then, to relate $y_{P'}$ and $z_{P'}$ to the variables x and θ , the condition that \mathbf{AP}' and \mathbf{AQ}' are always collinear is enforced. The components of \mathbf{AQ}' projected in $\{x, y, z\}$ are

$$\mathbf{AQ}' = (R - u_F(R))\mathbf{i} + \frac{c}{2}(\cos \theta - 1)\mathbf{j} + \frac{c}{2}\sin \theta \mathbf{k} \quad (4)$$

From the inextensible cables assumption, it can be deduced that $\|\mathbf{AQ}'\| = R$, hence,

$$u_F(R) = R - \sqrt{R^2 - \frac{c^2}{2}(1 - \cos \theta)} \quad (5)$$

Since \mathbf{AP}' and \mathbf{AQ}' are collinear, we must have

$$\mathbf{AP}' \times \mathbf{AQ}' = \mathbf{0} \quad (6)$$

which results in a system of three equations. Two of these three equations are independent and give expressions for $y_{P'}$ and $z_{P'}$ as

$$y_{P'} = \frac{c(R - x + x \cos \theta)}{2R} \quad (7)$$

$$z_{P'} = \frac{cx \sin \theta}{2R} \quad (8)$$

Finally, substituting Eq. (7) into Eq. (3), the foreshortening at any location x is given by

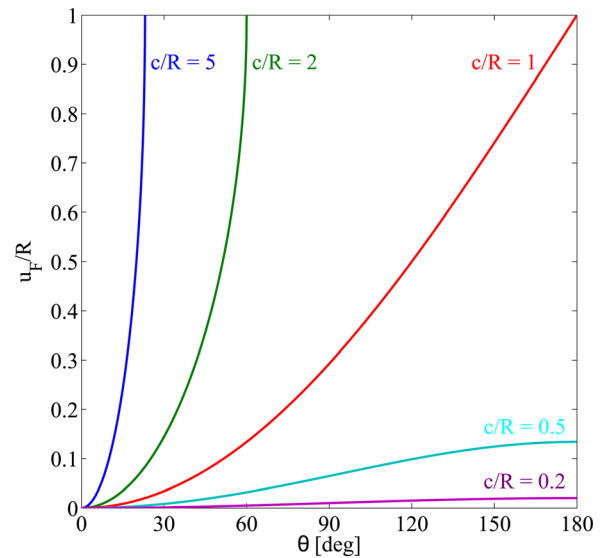


Fig. 2 Kinematic foreshortening induced in a twisted trapeze, for various chord over length ratios

$$u_F(x) = x - \frac{x}{R} \sqrt{R^2 - \frac{c^2}{2}(1 - \cos \theta)} \quad \text{for } \theta \in [0; \pi] \quad (9)$$

This formula is geometrically exact and valid for any arbitrarily large angle θ . However, when $\theta = \pi$, the two cables come in contact and the kinematics of the trapeze changes. If one assumes that the diameter of the cables is infinitesimally small, then the motion of the trapeze outboard of the contact point is a pure rotation about a fixed point, which induces no additional foreshortening.

The tip displacement $u_F(R)$ normalized by the trapeze length R is plotted in Fig. 2 as a function of the tip twist θ , for various trapeze geometries. It can be seen that the axial foreshortening, and consequently the trapeze effect, increases as c/R increases. In addition, for $c/R > 1$, the maximum twist angle at the end of the trapeze is kinematically limited to a value less than 180 deg. Note also that for $c = R$, the total foreshortening when $\theta = 180$ deg is equal to the trapeze length.

In the case treated above, the two cables, when deformed, are free to penetrate a virtual cylinder of diameter equal to the width at the root of the trapeze. However, if instead of a trapeze, a ribbon is considered, then the deformation of each longitudinal fiber is constrained because of the presence of neighboring fibers. In Sec. 2.1.2, the kinematics of a thin flexible ribbon in torsion is investigated.

2.1.2 Thin Ribbon. A thin ribbon composed of an infinite number of fibers, aligned parallel to each other, is considered. When a torque is applied at a given section of the ribbon, that section rotates about a point called the torsional center. The loci of torsional centers at every section constitute the torsional axis [10]. In the case of a ribbon of rectangular cross section under pure torsion, the torsional axis is coincident with the middle axis. Hence, when the ribbon is twisted, the central fiber remains straight while the outer fibers take a helicoidal shape, as shown in Fig. 3. The radius of the helix made by a deformed fiber is equal to the distance from the fiber to the torsional axis, denoted by η in Fig. 3. If the end of the ribbon is prevented from warping, then tensile stresses are created in the outer fibers, and compressive stresses occur in the inner fibers. One fiber on both sides of the torsional axis is strain-free. Enforcing the free-end condition at the tip of the ribbon, it can be shown that the resultant normal stress must be zero. From this condition, the foreshortening of the torsional axis can be deduced. In the following derivation, the

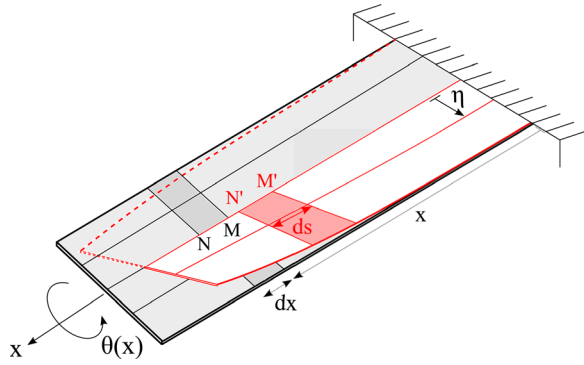


Fig. 3 Undeformed and deformed shape of a thin ribbon in torsion

foreshortening displacement $u_F(x)$ is expressed in terms of the twist angle $\theta(x)$.

The compressive strain in the central fiber, coincident with the torsional axis (see Fig. 3), is given by

$$\varepsilon_0 = \frac{\|M'N'\| - \|MN\|}{\|MN\|} \quad (10)$$

$$= \frac{[(x + dx + u_F(x + dx)) - (x + u_F(x))] - dx}{dx} \quad (11)$$

Taking the limit of Eq. (11) as $dx \rightarrow 0$ gives

$$\varepsilon_0 = u'_F(x) \quad (12)$$

In addition, the strain in the fiber located at a distance η from the torsional axis is

$$\varepsilon(\eta) = \frac{ds - dx}{dx} \quad (13)$$

Using the parametric expression for the length of a helix, it can be shown that

$$ds = [\theta'(x + dx) - \theta'(x)]\sqrt{\eta^2 + b^2} \quad (14)$$

where b is the pitch of the helix. Thus, for small dx

$$\varepsilon(\eta) = \theta'(x)\sqrt{\eta^2 + b^2} - 1 \quad (15)$$

The pitch of the helix can be expressed as a function of ε_0 as

$$b = \frac{\varepsilon_0 + 1}{\theta'} \quad (16)$$

Therefore, Eq. (13) becomes

$$\varepsilon(\eta) = \sqrt{(\theta'\eta)^2 + (\varepsilon_0 + 1)^2} - 1 \quad (17)$$

which, for small strains, further simplifies as

$$\varepsilon(\eta) = \varepsilon_0 + \frac{1}{2}\theta'^2\eta^2 + \mathcal{O}(\varepsilon_0^2) \quad (18)$$

Since the ribbon is under pure torsion, the net axial force integrated over the ribbon cross section should be zero. Hence,

$$\int_{-c/2}^{c/2} \varepsilon(\eta)d\eta = 0 \quad (19)$$

which gives the strain in the central fiber as

$$\varepsilon_0 = -\frac{c^2}{12} \frac{\theta'^2}{2} \quad (20)$$

Finally, substituting Eq. (20) into Eq. (12), it can be shown that

$$u_F(x) = -\int_0^x \frac{c^2}{12} \frac{\theta'^2}{2} dx \quad (21)$$

Note that the neutral fiber (or strain free fiber) is located at a distance equal to $\sqrt{c^2/12}$ on each side of the torsional axis, which corresponds to the radius of gyration of the ribbon about its midline.

Generalizing the above derivation to the case of a ribbon of thickness t , it is straightforward to show that the longitudinal strain in a fiber located at distances η and ξ from the torsional axis, in the edgewise and flatwise directions, respectively, is

$$\varepsilon(\eta, \xi) = \varepsilon_0 + \frac{1}{2}\theta'^2(\eta^2 + \xi^2) \quad (22)$$

In addition, in the absence of net axial force, the strain becomes

$$\varepsilon(\eta, \xi) = \frac{\theta'^2}{2}(\eta^2 + \xi^2 - k_A^2) \quad (23)$$

where k_A is the polar radius of gyration of the ribbon about the torsional axis. For a ribbon of rectangular cross section

$$k_A^2 = \frac{c^2 + t^2}{12} \quad (24)$$

Finally, the expression for the foreshortening due to the trapeze effect is

$$u_F(x) = -\int_0^x k_A^2 \frac{\theta'^2}{2} dx \quad (25)$$

The kinematic relationship derived above can be used to compute the restoring torque due to the trapeze effect.

2.2 Restoring Torque. The longitudinal tensile stress in a fiber of the twisted ribbon shown in Fig. 3, subjected to zero net axial force, can be deduced from Eq. (23) as

$$\sigma(\eta, \xi) = E \frac{\theta'^2}{2} (\eta^2 + \xi^2 - k_A^2) \quad (26)$$

where E is the Young's modulus of the fiber. If the cross section of the ribbon is rectangular, the maximum tensile stress occurs in the fiber most distant from the torsional axis ($\eta = c/2$, $\xi = t/2$). Thus,

$$\sigma_{\max} = \frac{E\theta'^2(c^2 + t^2)}{12} \quad (27)$$

The minimum stress (compressive stress) occurring in the middle fiber ($\eta = 0$, $\xi = 0$) is

$$\sigma_{\min} = -\frac{E\theta'^2(c^2 + t^2)}{24} \quad (28)$$

The magnitude of these longitudinal stresses can be compared to the maximum shear stress which also arises in the twisted ribbon, predicted by Saint-Venant theory. For a narrow rectangular cross section, it can be shown that [11]

$$\tau_{\max} = tG\theta' \quad (29)$$

Substituting θ' into Eqs. (27) and (28), we obtain

$$\sigma_{\max} = \frac{E\tau_{\max}^2}{12G^2} \left(\frac{c^2}{t^2} + 1 \right) \quad (30)$$

$$\sigma_{\min} = -\frac{E\tau_{\max}^2}{24G^2} \left(\frac{c^2}{t^2} + 1 \right) \quad (31)$$

As noted by Timoshenko in Ref. [11], the above longitudinal stresses, which arise due to the trapeze effect, are proportional to τ_{\max}^2 ; hence, the importance of these stresses increases with increasing τ_{\max} , i.e., with increasing angle of twist. For most metallic materials, such as aluminum or steel, τ_{\max} is always very small in comparison with G , and the magnitude of σ_{\max} is therefore small in comparison with τ_{\max} . However, for a composite material with low shear modulus on the order of a few megapascals, τ_{\max} may be of the same order of magnitude as G . Hence, σ must be taken into consideration. Note also that the ratio E/G is approximately equal to 2.6 for isotropic and homogeneous materials with a Poisson's ratio of 0.3. But it can be significantly larger for anisotropic materials, around 21 for a carbon/epoxy (AS4/3501-6) unidirectional composite. Finally, Eq. (30) shows that the magnitude of σ_{\max} , or in other words the importance of the trapeze effect, increases when $c \gg t$.

The longitudinal stresses in the deformed fibers create a restoring torque about the midline of the ribbon, as shown in Fig. 4. The projection of σ on a plane perpendicular to the midline is

$$\sigma' = \sigma \sin \gamma \quad (32)$$

where γ is the angle the displaced fiber makes with the vertical. From Fig. 4, it can be seen that

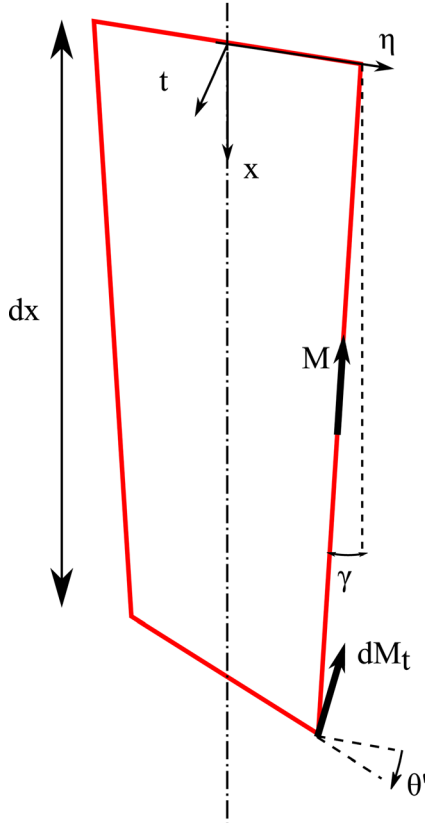


Fig. 4 Restoring torque induced by longitudinal stresses in the fibers

$$\sin \gamma = \sqrt{\eta^2 + \xi^2} \theta' \quad (33)$$

Hence, the restoring torque produced by the stretched fiber, about the midline is

$$dM_t = E \frac{\theta'^3}{2} (\eta^2 + \xi^2 - k_A^2) (\eta^2 + \xi^2) d\eta d\xi \quad (34)$$

Integrating over the ribbon cross section, the torque due to the trapeze effect is

$$M_t = E \frac{\theta'^3}{2} (B_1 - Ak_A^4) \quad (35)$$

where $B_1 = \iint_A (\eta^2 + \xi^2)^2 dA$. Combining this torque with the torque T_{SV} due to the shear stress (predicted according to Saint-Venant's theory), the total restoring torque acting on the ribbon is

$$M_t = T_{SV} + E \frac{\theta'^3}{2} (B_1 - Ak_A^4) \quad (36)$$

This last result was specialized by Timoshenko [11] and Biot [12,13] to the case of a narrow rectangular cross section and it was shown that in this case

$$\begin{aligned} M_t &= \frac{ct^3}{3} G\theta' + \frac{1}{360} Et c^5 \theta'^3 \\ &= \frac{ct^3}{3} G\theta' \left(1 + \frac{1}{120} \frac{E}{G} \frac{c^4}{t^2} \theta'^2 \right) \end{aligned} \quad (37)$$

It can be seen that when $c \gg t$ and the angle of twist is large, the restoring torque associated with the trapeze effect may contribute an important portion of the total torque.

Finally, the influence of a uniform axial load (equal to $\sigma_0 A$) on the restoring torque due to the trapeze effect is considered. With this new boundary condition, the equilibrium equation given by Eq. (19) becomes

$$\iint_A E\varepsilon(\eta, \xi) dA = \sigma_0 A \quad (38)$$

from which

$$\varepsilon_0 = \frac{\sigma_0}{E} - k_A^2 \frac{\theta'^2}{2} \quad (39)$$

The expression for the longitudinal stress becomes

$$\sigma(\eta, \xi) = E \frac{\theta'^2}{2} (\eta^2 + \xi^2 - k_A^2) + \sigma_0 \quad (40)$$

And the total restoring torque acting on the ribbon cross section, including the Saint-Venant's torque T_{SV} , is

$$M_t = T_{SV} + E \frac{\theta'^3}{2} (B_1 - Ak_A^4) + \sigma_0 Ak_A^2 \theta' \quad (41)$$

Consequently, it can be seen from Eq. (41) that the action of the tensile stress σ_0 is to increase the restoring torque and reduce the twisting length θ' . In addition, we note that the untwisting effect due to the axial load is purely linear in the twist per unit length θ' , unlike the restoring torque due to the change in fibers shape and geometry, which is proportional to θ'^3 . Finally, the Saint-Venant restoring torque is also a linear term in θ' .

In summary, for a ribbon with low shear modulus and small thickness-to-width ratio, non-negligible longitudinal stresses arise in the deformed fibers as a result of the trapeze effect. In addition, the restoring torque produced by these stresses is nonlinear. Finally, an external axial force tends to decrease the twist of the ribbon in a linear fashion.

Note that these results were developed for the case of a homogeneous twisted ribbon subjected to an axial load resulting in a uniform axial stress state. Under these conditions, it was assumed that the torsional axis is coincident with the midline of the ribbon. In Sec. 2.3, it is shown that the torsional axis is actually defined by the centroid of the axial stress field at each spanwise location.

2.3 Position of the Torsional Axis. The objective is to compute the locus of torsional centers for the general case where the axial stress field is not distributed uniformly along the cross section of the ribbon. Accordingly, we consider the structure shown in Fig. 5, comprised a soft ribbon of rectangular cross section rotating at the angular velocity Ω , and stiffened by centrifugal forces. At the root, elastic displacements and rotations are prevented. At the tip, a solid rod is secured such that its longitudinal axis is parallel to the width of the ribbon, defined by the body-fixed axis η . The position of the center of gravity of the tip body along the η -axis relative to the midline of the ribbon (x -axis) is defined by the parameter $\bar{\eta}_m$. Additionally, the torsional center of each cross section is assumed to be located at a distance $\bar{\eta}_c(x)$ from the x -axis. For clarity, the locus of torsional centers is shown by a straight dashed-line in Fig. 5. However, the following analysis is derived for the general case, and does not assume that the torsional axis is straight.

From equilibrium, the internal normal force and bending moment acting at a distance x from the axis of rotation are

$$N(x) = m_0 \Omega^2 \frac{R^2 - x^2}{2} + M_m \Omega^2 R \quad (42)$$

$$M(x) = -M_m \Omega^2 \bar{\eta}_m x \quad (43)$$

where m_0 is the mass of the ribbon per unit length and M_m is the tip mass.

Using the superposition principle, the axial stress at any location x and distance $\bar{\eta}$ from the midline of the ribbon is

$$\sigma(x, \bar{\eta}) = \frac{N(x)}{A} - \frac{M(x)\bar{\eta}}{I_{\bar{\eta}}} \quad (44)$$

In addition, it was shown in Eq. (32) that the tangential component of the stress in a deformed ribbon fiber responsible for a restoring torque about the torsional axis is

$$\sigma_t(x, \eta) = \sigma(x, \eta) \sin \gamma \quad (45)$$

$$= \sigma(x, \bar{\eta})(\bar{\eta} - \bar{\eta}_c) \theta' \quad (46)$$

where η is the distance from the torsional axis to the fiber and γ is the angle made by the deformed fiber relative to the torsional axis. Multiplying Eq. (46) by the width of a fiber, the force responsible for the restoring torque due to the trapeze effect, directed perpendicularly to the η -axis, is obtained as

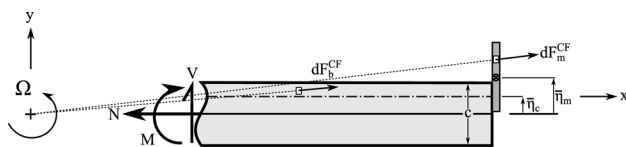


Fig. 5 Free-body diagram of the forces and moments applied to a rotating ribbon with tip mass

$$dF_t(x, \bar{\eta}) = \sigma(x, \bar{\eta})(\bar{\eta} - \bar{\eta}_c) \theta' d\bar{\eta} \quad (47)$$

But it can be seen from Fig. 5 that the resultant transverse force along the direction perpendicular to the η -axis equals zero. Therefore,

$$\int_{-c/2}^{c/2} dF_t(x, \bar{\eta}) d\bar{\eta} = 0 \quad (48)$$

Substituting Eqs. (44) and (47) into Eq. (48), we obtain

$$\bar{\eta}_c(x) = -\frac{M(x) A c^2}{N(x) I_{\bar{\eta}} 12} \quad (49)$$

Thus, Eq. (49) shows that the torsional center is coincident with the centroid of the axial stress distribution, which is derived as

$$\bar{\eta}_c(x) = \frac{\int_{-c/2}^{c/2} \bar{\eta} \sigma(x, \bar{\eta}) d\bar{\eta}}{\int_{-c/2}^{c/2} \sigma(x, \bar{\eta}) d\bar{\eta}} \quad (50)$$

$$= -\frac{M(x) A c^2}{N(x) I_{\bar{\eta}} 12} \quad (51)$$

For a given set of design parameters ($m_0 = 13 \text{ g}\cdot\text{m}^{-1}$, $M_m = 2 \text{ g}$, $\Omega = 1200 \text{ rpm}$, $R = 0.23 \text{ m}$), we can plot the centroid of the axial stress field along the span of the ribbon (see Fig. 6). First, it can be seen from Eq. (49) that the result is independent of the rotational speed. Second, one can verify that the torsional axis passes through the midline of the ribbon at the root and the center of gravity of the tip mass. Finally, note from Eq. (49) that the shape of the curve describing the torsional axis is a second-order polynomial in x ; if the mass of the ribbon was negligible compared to the tip mass (i.e., $m_0 \sim 0$ in Eq. (42)), then it is trivial to show that the torsional axis would be a straight line passing through the midline of the ribbon at the root and the center of gravity of the tip mass. The latter outcome was also observed, but not proven, by Roeseler in Ref. [14].

The result shown by Eq. (50) and plotted in Fig. 6 is a new contribution of this paper. A direct consequence of this result is a new definition of the EA (which is conventionally defined as the spanwise locus of elastic centers) for slender beams subjected to combined axial and transverse forces. Let us recall that for the case of a beam under pure shear, the elastic center at each cross section is coincident with the shear center, which is the point where transverse forces must be applied to induce pure bending and no twist. In contrast, when axial loading is combined with the transverse forces, the elastic center is shifted to the centroid of the axial stress field at each spanwise location, point about which the cross section twists.

When modeling rotating slender members, such as helicopter blades for instance, it is typical to make the Euler–Bernoulli beam assumptions. In this case, the one-dimensional beam elements are assumed to coincide with the blade EA. In Sec. 3, we investigate the effect of the new modeling of the EA described above on the predictions of deformation and natural frequencies.



Fig. 6 Spanwise locus of centroid of the axial stress field

3 Analytical Study

An analytical model was developed to predict the steady-state deformation and the natural frequencies of the soft ribbon with tip mass, rotating in vacuum, shown in Fig. 5.

3.1 Description of the Model. Equations of motion were derived using Hamilton's principle, written for N degrees of freedom as

$$\text{if } \delta q_i|_{t_1} = \delta q_i|_{t_2} = 0, (i = 1, \dots, N) \text{ then}$$

$$\int_{t_1}^{t_2} (\delta T - \delta U) dt = 0 \quad (52)$$

where δq_i are generalized coordinates and δT and δU are the variations in the kinetic energy and strain energy. For the structure shown in Fig. 5, Eq. (52) becomes

$$\int_{t_1}^{t_2} [(\delta T - \delta U)_b + (\delta T)_m] dt = 0 \quad (53)$$

where the subscripts ()_b and ()_m indicate energies of the ribbon and the tip mass, respectively.

By modeling the ribbon as an Euler–Bernoulli beam, Eq. (53) becomes one dimensional in space. Furthermore, the beam deformations are described by the axial displacement of the EA u and the angle of twist θ . In previous analyses derived for stiff rotating beams [15–17], the EA was commonly chosen to be passing through the locus of shear center at each cross section of the beam. The motivation for this approach was to decouple twist deformations from the action of transverse loads. In the present model, the EA is defined as the spanwise locus of centroid of the axial stress field. Introducing $\bar{\theta}(x) = \theta_0 + \theta(x)$ as the total pitch angle at the spanwise location x , it can be shown (see Ref. [18]) that to second-order

$$\begin{aligned} \int_{t_1}^{t_2} (\delta T)_b dt &= \int_{t_1}^{t_2} \int_R \left[\{m_0 \Omega^2 x - m_0 \ddot{u} - 2m_0 \Omega \dot{\theta} d_\eta \sin \bar{\theta}\} \delta u \right. \\ &\quad + \left\{ 2m_0 \Omega \dot{u} d_\eta \sin \bar{\theta} - \frac{1}{2} m_0 \Omega^2 (k_{m\xi}^2 - k_{m\eta}^2) \sin 2\bar{\theta} \right. \\ &\quad \left. \left. - m_0 k_m^2 \ddot{\theta} \right\} \delta \theta \right] dx dt \quad (54) \end{aligned}$$

$$\begin{aligned} \int_{t_1}^{t_2} (\delta U)_b dt &= \int_{t_1}^{t_2} \int_R \left[\left\{ EA u' + EA \frac{k_A^2}{2} \theta'^2 \right\} \delta u' \right. \\ &\quad \left. + \left\{ EA k_A^2 u' \theta' + \left(\frac{EB_1}{2} \right) \theta'^3 + GJ \theta' \right\} \delta \theta' \right] dx dt \quad (55) \end{aligned}$$

$$\begin{aligned} \int_{t_1}^{t_2} (\delta T)_m dt &= \int_{t_1}^{t_2} \left[\{M_m \Omega^2 R - 2M_m \Omega \dot{\theta}_m \eta_m \sin \bar{\theta}_m\} \delta u_m \right. \\ &\quad + \left\{ 2M_m \Omega \dot{u}_m \eta_m \sin \bar{\theta}_m - M_m \ddot{\theta}_m \left(\eta_m^2 + \frac{c^2}{12} \right) \right. \\ &\quad \left. \left. - M_m \Omega^2 \left(\eta_m^2 + \frac{c^2}{12} \right) \sin \bar{\theta}_m \cos \bar{\theta}_m \right\} \delta \theta_m \right] dt \quad (56) \end{aligned}$$

Then, the steady-state deformations are obtained by solving the time-invariant part of Eq. (53), using the finite element method. Additionally, the natural frequencies are computed by perturbing the equations of motion about the steady-state and by performing an eigenanalysis of the free response.

3.2 Results and Discussion. The objective of the analysis presented in this paper is to investigate the effect of two different approaches regarding the modeling of the EA of a ribbon

subjected to combined axial and transverse loads, on the predictions of deformation and natural frequencies. First, the predictions obtained when the EA is assumed to pass through the shear center (which is located at the midline of the uniform ribbon) are presented. Then, these predictions are compared to that obtained when the EA is assumed to pass through the centroid of the axial stress field.

A 50 cm long, 5 cm wide, flexible rotating ribbon, stiffened by the centrifugal forces acting on a tip body was studied. The ribbon was assumed to be made of unidirectional fibers of Young's modulus equal to 200 GPa, aligned in the spanwise direction. The tip body was placed such that its center of gravity was not coincident with the ribbon midline, effectively creating a nonuniform distribution of axial stresses at each cross section. In addition, the mass of the tip body was chosen to be an order of magnitude greater than the mass of the ribbon. The whole assembly was assumed to be rotating at 1500 rpm, in vacuo. Additional parameters are given in Table 1.

The deformation and the natural frequencies of the ribbon with tip mass were predicted using the numerical model described in Sec. 3.1. The results were obtained for root pitch angles (angles between the horizontal plane and the η -axis) varying from 0 to 90 deg. The centroid of the axial stress field was computed according to Eq. (49), in which were substituted the following expressions:

$$\begin{aligned} N(x) &= \int_x^R \int_{-c/2}^{c/2} \rho t \Omega^2 \sqrt{\frac{(\chi + u)^2 + \eta^2 \cos^2 \bar{\theta}}{(\chi + u)^2 + \eta^2}} (\chi + u) d\eta d\chi \\ &\quad + \int_{\bar{\eta}_m - \frac{L_m}{2}}^{\bar{\eta}_m + \frac{L_m}{2}} \frac{M_m}{L_m} \Omega^2 \sqrt{\frac{(R + u_R)^2 + \eta^2 \cos^2 \bar{\theta}_R}{(R + u_R)^2 + \eta^2}} (R + u_R) d\eta \quad (57) \end{aligned}$$

$$\begin{aligned} M(x) &= - \int_x^R \int_{-c/2}^{c/2} \rho t \Omega^2 \sqrt{\frac{(\chi + u)^2 + \eta^2 \cos^2 \bar{\theta}}{(\chi + u)^2 + \eta^2}} \eta (x + u_x) d\eta d\chi \\ &\quad - \int_{\bar{\eta}_m - \frac{L_m}{2}}^{\bar{\eta}_m + \frac{L_m}{2}} \frac{M_m}{L_m} \Omega^2 \sqrt{\frac{(R + u_R)^2 + \eta^2 \cos^2 \bar{\theta}_R}{(R + u_R)^2 + \eta^2}} \eta (x + u_x) d\eta \quad (58) \end{aligned}$$

where $u_R = u(R)$ and $\bar{\theta}_R = \bar{\theta}(R)$. Note that Eqs. (57) and (58) are generalizations of Eqs. (42) and (43) which include the geometric changes due to the elastic deformations (extension and twist). However, it can be seen that for a slender ribbon ($\eta \ll R$), Eqs. (42) and (43) are very good approximations.

Figure 7 shows the variation of internal normal force and bending moment along the span of the rotating ribbon. We can verify that the normal force at the tip is equal to the axial load due to the centrifugal forces acting on the tip mass (i.e., the second term of Eq. (42)). In addition, the position of the centroid of the axial

Table 1 Parameters of the simulation

Geometric properties	
Length (m)	0.5
Width (m)	0.05
Thickness (m)	0.001
Material properties	
Linear density (kg·m ⁻¹)	0.01
Young's modulus (GPa)	200
Tip mass properties	
M_m (kg)	0.05
L_m (m)	0.05
$\bar{\eta}_m$ (m)	0.025
Operating conditions	
Ω (rpm)	1500
Environment	in vacuo

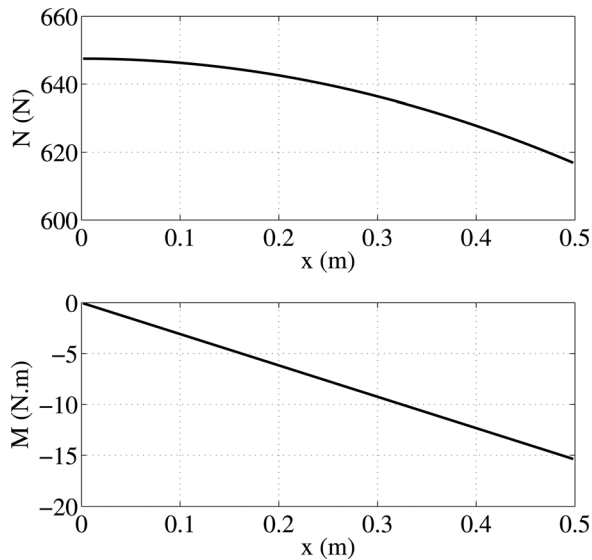


Fig. 7 Spanwise variation of internal normal force N and internal bending moment M

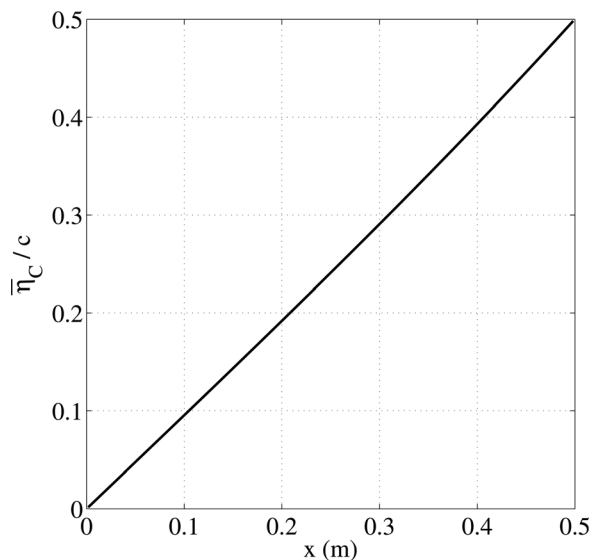


Fig. 8 Spanwise locus of the EA relative to the middle axis of the ribbon

stress field relative to the middle axis is plotted in Fig. 8. In this case, the EA appears to be almost linear in the spanwise coordinate x , which is due to the large magnitude of the tip mass relative to the mass of the ribbon.

The twist and the elongation at the tip of the ribbon are plotted in Figs. 9 and 10, respectively, for various root pitch angles, and for both cases where the EA is assumed to be passing through the shear centers or the centroids of the axial stress field. It can be seen that by assuming the EA to pass through the shear centers, the tip twist is generally overpredicted by a factor of 2 for small root pitch angles and over 2.5 for large root pitch angles. In addition, while the tip twist appears to vary linearly with the increase in root pitch for the case where the EA is coincident with the locus of shear centers, it is asymptotic to a limit approximately equal to -15 deg when the EA is coincident with the centroids of the axial stress field.

Similar observations can be made regarding the variation of tip axial deflection shown in Fig. 10. When the root pitch angle equals 0 deg, the ribbon is untwisted, therefore the foreshortening

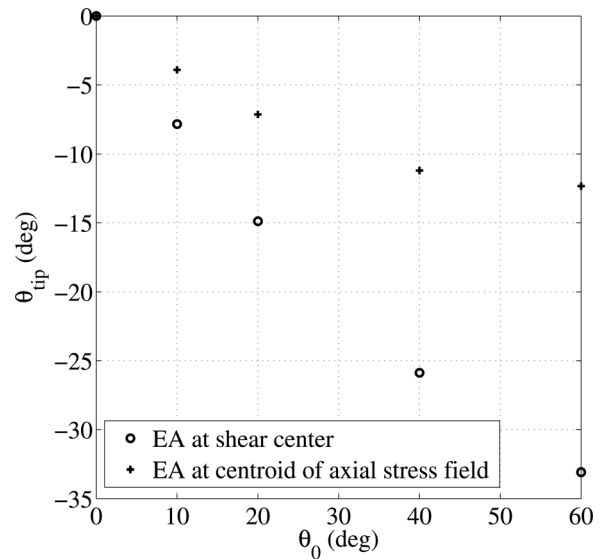


Fig. 9 Variation of the tip twist with root pitch angles

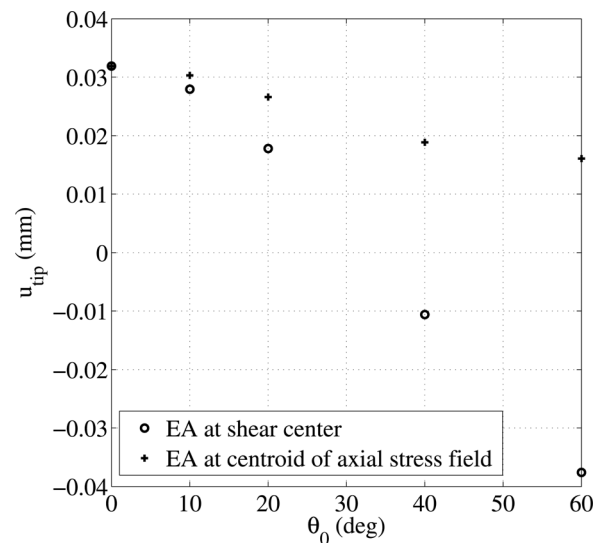


Fig. 10 Variation of the tip axial deflection with root pitch angles

of the EA due to the trapeze effect vanishes and the elongation is solely due to elastic deformation. In this case, both simulations predict a tip elongation equal to $32 \mu\text{m}$. As the root pitch increases, the ribbon experiences twist deformations which induce foreshortening (i.e., negative axial displacement) because of the trapeze effect. Since the total elongation is the result of the sum of the elastic elongation, which is constant, and the kinematic extension–torsion coupling due to the trapeze effect, we can observe that the elongation varies with the root pitch angle in a similar fashion as the twist variation with root pitch.

The total pitch angle $\bar{\theta}$ is plotted as a function of the spanwise coordinate x in Fig. 11. When θ_0 equals 0 or 90 deg, the centrifugal twisting moment acting on the ribbon and the tip mass vanishes, thus the predictions show zero twist. As the root pitch increases, it can be seen that in the case where the EA is passing through the shear centers, the spanwise variation of elastic twist is linear. In contrast, when the EA is defined as the locus of centroid of the axial stress field, the elastic twist distribution flattens out toward the tip of the ribbon.

For completeness, the spanwise variation of axial elongation is plotted in Fig. 12 for the case where the EA is passing through the

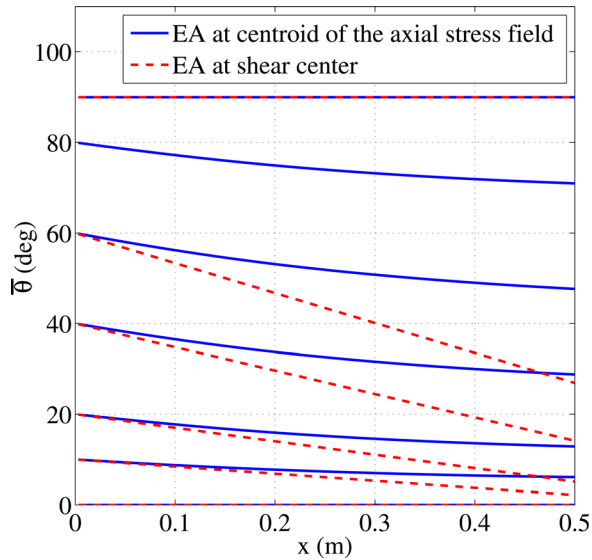


Fig. 11 Spanwise variation of total pitch angles

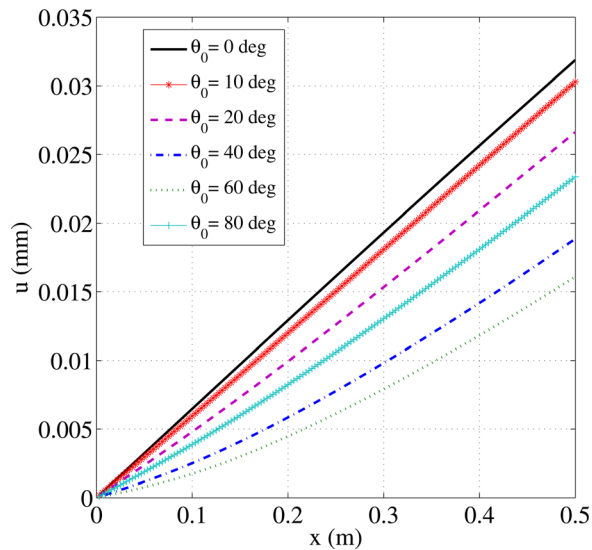


Fig. 12 Spanwise variation of axial elongation (EA at centroid of the axial stress field)

centroids of the axial stress field. The solid black curve corresponding to zero root pitch angle shows the elastic elongation experienced by the untwisted ribbon. As the twist increases, the total elongation decreases as explained earlier. It is interesting to note that the smallest magnitudes of elongation are obtained for the case where $\theta_0 = 60$ deg. When $\theta_0 = 80$ deg, the magnitude of the centrifugal nose-down moment, which is proportional to $\sin(2\bar{\theta})$ [19] decreases. Consequently, the extension–torsion coupling effect which induces the foreshortening also decreases.

Finally, the natural frequencies corresponding to the first five modes of vibration of the rotating ribbon were predicted (see Fig. 13). It can be seen that in the case where the EA is assumed to be coincident with the shear centers, natural frequencies are always overpredicted. Although the error relative to the frequencies computed when the EA is passing through the centroids of the axial stress field is negligible for root pitch angles less than 15 deg, it reaches up to 60% for large pitch angles above 40 deg.

We can also note that the mode shapes corresponding to the first five modes of vibration, for both approaches regarding the modeling of the EA, exhibit pure extension–torsion coupled

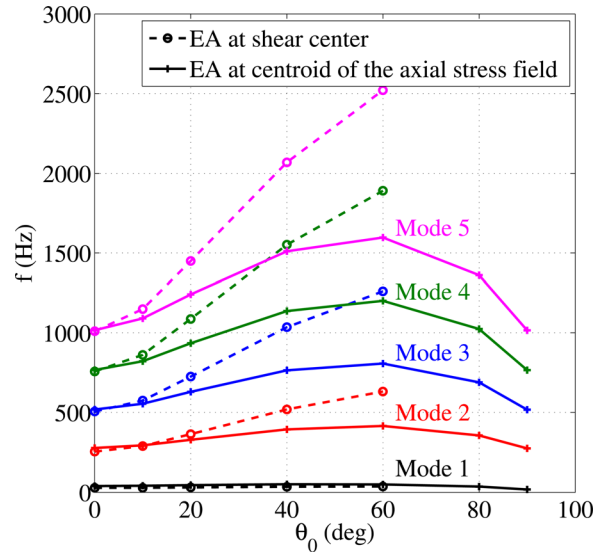


Fig. 13 Natural frequencies of the flexible ribbon rotating at 1500 rpm

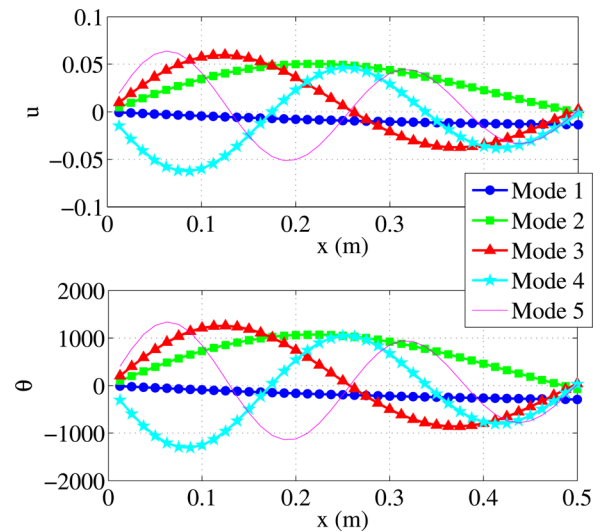


Fig. 14 Natural mode shapes

motions (see Fig. 14). Therefore, it can be concluded that these modes of vibration are all associated with to the trapeze effect.

4 Conclusion

An analytical investigation of the trapeze effect acting on flexible twisted ribbons was presented. This effect, characterized by an increase of the torsional rigidity of a member subjected to an axial load, is a consequence of the geometric change of direction of the twisted fibers in the member.

First, the amount of foreshortening due to the extension–torsion coupling was derived as a function of the twist angle. In addition, the magnitude of the restoring torque associated with the trapeze effect was computed for a ribbon with arbitrary cross section. In particular, it was shown that for a ribbon with low shear modulus and small thickness-to-width ratio, the restoring torque produced by longitudinal stresses in the deformed fibers is of the same order of magnitude as the torque induced by the action of the shear stresses, classically predicted by Saint–Venant’s theory.

Additionally, this paper showed that torsional centers, which are the points at each cross section about which the ribbon twists

when subjected to a torque, are coincident with the centroids of the axial stress field. More generally, it was shown that transverse forces must also be applied at the centroid of the axial stress field, for the ribbon to experience pure bending and no twist. This result redefines the location of the EA of a slender member subjected to combined axial force, transverse force and a torque.

A numerical model was developed to compute the steady-state deformation and natural frequencies of a ribbon whose EA is defined by the centroids of the axial stress field. For comparison, the deformation and natural frequencies obtained when the EA passes through the shear centers were also calculated. It was found that a model which assumes the EA to be coincident with the shear centers overpredicts the tip twist by a factor of 2 for small twist angles, and up to 2.5 for large twist deformations. In addition, the twist appeared to decrease linearly with both the increase in root pitch angles and the spanwise coordinate when the EA was coincident with the locus of the shear centers. In contrast, when the EA was defined by the centroids of the axial stress field, the slope of the spanwise twist distribution decreased with increasing root pitch.

Finally, it was found that the natural frequencies of the twisted ribbon computed by the model which assumed EA and shear centers to be coincident were well predicted for small twist deformations, less than 15 deg. For larger twist angles, the error relative to the predictions obtained when the EA passed through the centroids of the axial stress field was up to 60%.

Nomenclature

A	= cross-sectional area of ribbon (m^2)
B_1	= cross-sectional constant (m^6)
c	= width of ribbon (m)
d_η	= edgewise distance from torsional center to mass centroid (m)
E	= Young's modulus (Pa)
G	= shear modulus (Pa)
I_ξ	= area moment of inertia about the torsional axis (m^4)
J	= polar moment of inertia about the torsional axis (m^4)
k_A	= polar radius of gyration about torsional axis (m)
k_m	= mass radius of gyration about torsional axis (m)
$k_{m\eta}, k_{m\xi}$	= mass radii of gyration about η and ξ axes (m)
L_M	= length of the tip mass (m)
M	= internal bending moment (N·m)
M_m	= tip body mass (kg)
M_η	= restoring torque (N·m)
m_0	= mass of ribbon per unit length ($\text{kg}\cdot\text{m}^{-1}$)
N	= internal normal force (N)
R	= length of ribbon (m)
t	= thickness of ribbon (m)
T	= kinetic energy (N·m)
T_{SV}	= restoring torque predicted by Saint-Venant's theory (N·m)
u	= axial displacement (m)
U	= strain energy (N·m)
u_F	= axial displacement associated with foreshortening (m)
ε	= longitudinal strain
η	= edgewise distance from torsional axis (m)
$\bar{\eta}$	= edgewise distance from midline of ribbon (m)

$\bar{\eta}_c$	= edgewise distance from midline to torsional axis (m)
η_m	= edgewise distance from torsional axis to center of gravity of tip body (m)
$\bar{\eta}_m$	= edgewise distance from midline to center of gravity of tip body (m)
θ	= twist angle (rad)
$\bar{\theta}$	= local pitch angle ($\bar{\theta} = \theta_0 + \theta$) (rad)
θ_0	= root pitch angle (rad)
ζ^c	= flatwise distance from torsional axis (m)
ζ	= flatwise distance from midline of ribbon (m)
σ	= longitudinal stress (Pa)
τ	= shear stress
Ω	= angular velocity ($\text{rad}\cdot\text{s}^{-1}$)

References

- [1] Campbell, A., 1911, "On Vibration Galvanometer With Unifilar Torsional Control," *Proc. Phys. Soc. London*, **25**(1), pp. 203–205.
- [2] Pealing, H., 1913, "On an Anomalous Variation of the Rigidity of Phosphor Bronze," *Philos. Mag. Ser. 6*, **25**(147), pp. 418–427.
- [3] Buckley, J. C., 1914, "The Bifilar Property of Twisted Strips," *Philos. Mag. Ser. 6*, **28**(168), pp. 778–787.
- [4] Houbolt, J. C., and Brooks, G. W., 1957, "Differential Equations of Motion for Combined Flapwise Bending, Chordwise Bending, and Torsion of Twisted Nonuniform Rotor Blades," Langley Aeronautical Laboratory, National Advisory Committee for Aeronautics, Langley Field, VA, Technical Note No. 3905.
- [5] Fulton, M. V., and Hodges, D. H., 1993, "Aeroelastic Stability of Composite Hingeless Rotor Blades in Hover—Part I: Theory," *Math. Comput. Modell.*, **18**(3–4), pp. 1–17.
- [6] Kaza, K. R. V., and Kielb, R. E., 1984, "Effects of Warping and Pretwist on Torsional Vibration of Rotating Beams," *ASME J. Appl. Mech.*, **51**(4), pp. 913–920.
- [7] Borri, M., and Merlini, T., 1986, "A Large Displacement Formulation for Anisotropic Beam Analysis," *Mecanica*, **21**(1), pp. 31–37.
- [8] Popescu, B., and Hodges, D. H., 1999, "Asymptotic Treatment of the Trapeze Effect in Finite Element Cross-Sectional Analysis of Composite Beams," *Int. J. Non Linear Mech.*, **34**(4), pp. 709–721.
- [9] Hodges, D. H., 2006, *Nonlinear Composite Beam Theory* (Progress in Astronautics and Aeronautics), American Institute of Aeronautics and Astronautics, Inc., Reston, VA, Vol. 213.
- [10] Young, W. C., Budynas, R. G., and Sadegh, A. M., 2012, *Roark's Formulas for Stress and Strain*, 8th ed., McGraw-Hill, New York.
- [11] Timoshenko, S. P., 1976, *Strength of Materials, Part II, Advanced Theory and Problems*, Van Nostrand Reinhold Company, Inc., New York.
- [12] Biot, M. A., 1939, "Non-Linear Theory of Elasticity and the Linearized Case for a Body Under Initial Stress," *Philos. Mag. Ser. 7*, **27**(183), pp. 468–489.
- [13] Biot, M. A., 1939, "Increase of Torsional Stiffness of a Prismatical Bar Due to Axial Tension," *J. Appl. Phys.*, **10**(12), pp. 860–864.
- [14] Roeseler, W. G., 1966, "The Effect of Ribbon Rotor Geometry on Blade Response and Stability," M.S. thesis, Massachusetts Institute of Technology, Cambridge, MA.
- [15] Hodges, D. H., and Dowell, E. H., 1974, "Nonlinear Equations of Motion for the Elastic Bending and Torsion of Twisted Nonuniform Rotor Blades," Ames Research Center and U.S. Army Air Mobility R&D Laboratory, Moffett Field, CA, Technical Note No. NASA TN D-7818.
- [16] Kaza, K. R. V., and Kvaternik, R. G., 1977, "Nonlinear Aeroelastic Equations for Combined Flapwise Bending, Chordwise Bending, Torsion and Extension of Twisted Nonuniform Rotor Blades in Forward Flight," Langley Research Center, National Aeronautics and Space Administration, Hampton, VA, Technical Memorandum No. NASA TM 74059.
- [17] Rosen, A., and Friedmann, P. P., 1978, "Nonlinear Equations of Equilibrium for Elastic Helicopter or Wind Turbine Blades Undergoing Moderate Deformation," Lewis Research Center, National Aeronautics and Space Administration, Cleveland, OH, Contractor Report No. NASA CR 159478.
- [18] Sicard, J., and Sirohi, J., 2014, "Modeling of the Large Torsional Deformation of an Extremely Flexible Rotor in Hover," *AAAA J.*, **52**(8), pp. 1604–1615.
- [19] Johnson, W., 1994, *Helicopter Theory*, Dover, New York.